ARTICLES
PUBLISHED ONLINE: 22 AUGUST 2010 | DOI: 10.1038/NMAT2812
nature materials

Combinatorial development of biomaterials for clonal growth of human pluripotent stem cells

Ying Mei[1†], Krishanu Saha[2†], Said R. Bogatyrev[1], Jing Yang[3], Andrew L. Hook[3], Z. Ilke Kalcioglu[4], Seung-Woo Cho[5], Maisam Mitalipova[2], Neena Pyzocha[2], Fredrick Rojas[1], Krystyn J. Van Vliet[4], Martyn C. Davies[3], Morgan R. Alexander[3], Robert Langer[1,6,7*], Rudolf Jaenisch[2,8*] and Daniel G. Anderson[1,6,7*]

Both human embryonic stem cells and induced pluripotent stem cells can self-renew indefinitely in culture; however, present methods to clonally grow them are inefficient and poorly defined for genetic manipulation and therapeutic purposes. Here we develop the first chemically defined, xeno-free, feeder-free synthetic substrates to support robust self-renewal of fully dissociated human embryonic stem and induced pluripotent stem cells. Material properties including wettability, surface topography, surface chemistry and indentation elastic modulus of all polymeric substrates were quantified using high-throughput methods to develop structure–function relationships between material properties and biological performance. These analyses show that optimal human embryonic stem cell substrates are generated from monomers with high acrylate content, have a moderate wettability and employ integrin $\alpha_v\beta_3$ and $\alpha_v\beta_5$ engagement with adsorbed vitronectin to promote colony formation. The structure–function methodology employed herein provides a general framework for the combinatorial development of synthetic substrates for stem cell culture.

Human pluripotent stem cells (both human embryonic stem (hES) and induced pluripotent stem (hiPS) cells) hold great promise for regenerative medicine[1–4] and human-disease modelling[5]. However, existing methods to grow human pluripotent stem cells are not well suited for genetic manipulation experiments and introduce animal components, increasing the risks of immune rejection. Present methods to grow hES and hiPS cells include growing them on a 'feeder' cell layer of mitotically inactivated mouse embryonic fibroblasts[1–3,6] (mEFs), and on 'feeder free' culture systems, composed of a variety of extracellular-matrix/serum proteins coated onto tissue-culture dishes[7–15] or synthetic materials[16–19] such as hyaluronic acid hydrogels. These have been reported to promote hES cell self-renewal when seeded at a suitably high cell density[9,16,17] (for example, $\sim 10^6$ cells ml^{-1} for the hydrogel) and have not been demonstrated to efficiently promote clonal growth of single hES cells (efficiencies typically $<10\%$). However, gene targeting in pluripotent stem cells necessitates clonal outgrowth of single cells to detect rare targeting events (1 in 10^5–10^6 cells) and requires selective growth of a correctly gene-targeted cell within a population of $>10^5$ cells[20–22]. Further, current human culture methods use either animal products or undefined components, which make it problematic for the potential transplantation applications[4]. Here we employed a high-throughput approach to engineer new culture substrates that could be used to clonally expand human pluripotent stem cells in a chemically defined, xeno-free, feeder-free manner.

To facilitate rapid synthesis and analysis of synthetic substrates, we manufactured cell-compatible, biomaterial microarrays[23,24]. Microarrays were prepared from 22 acrylate monomers with diversified hydrophobicity–hydrophilicity and crosslinking densities (Fig. 1a). The arrays were prepared by copolymerization between each of 16 'major' monomers (numbered 1–16) and each of six 'minor' monomers (lettered A–F) at six different ratios (100:0, 90:10, 85:15, 80:20, 75:25, 70:30 (v/v)) (Supplementary Fig. S1). In this way, arrays with 496 $[16 + (16 \times 5 \times 6)]$ different combinations were created, consisting of the major monomer (70–100%) and minor monomer (0–30%). These monomer mixtures were robotically deposited in triplicate on a non-cell adhesive layer of poly(2-hydroxyethyl methacrylate) covering conventional glass slides (75 mm × 25 mm), and then polymerized with a long-wave ultraviolet source.

We next used fluorescence-activated cell sorting of transgenic hES cells to ensure that hES cells were both dissociated from one another and undifferentiated in our assays (Fig. 1b). A transgenic green-fluorescent protein (GFP) reporter for Oct4 expression, a marker of pluripotent cells (Supplementary Fig. S2), was knocked in to the BG01 hES cell line and propagated under standard hES cell culture conditions using mEFs[25]. GFP$^+$ sorted hES

[1]Department of Chemical Engineering, Massachusetts Institute of Technology, 77 Massachusetts Avenue, Cambridge, Massachusetts 02139, USA, [2]The Whitehead Institute for Biomedical Research, 9 Cambridge Center, Cambridge, Massachusetts 02142, USA, [3]Laboratory of Biophysics and Surface Analysis, School of Pharmacy, The University of Nottingham, Nottingham, NG7 2RD, UK, [4]Department of Material Sciences and Engineering, Massachusetts Institute of Technology, 77 Massachusetts Avenue, Cambridge, Massachusetts 02139, USA, [5]Department of Biotechnology, Yonsei University, Seoul 120-749, Korea, [6]David H. Koch Institute for Integrative Cancer Research, Massachusetts Institute of Technology, 45 Carleton Street, Building E25-342, Cambridge, Massachusetts 02142, USA, [7]Harvard-MIT Division of Health Science Technology, Massachusetts Institute of Technology, 45 Carleton Street, Building E25-342, Cambridge, Massachusetts 02142, USA, [8]Department of Biology, Massachusetts Institute of Technology, 9 Cambridge Center, Cambridge, Massachusetts 02142, USA. †These authors contributed equally to this work. *e-mail: rlanger@mit.edu; jaenisch@wi.mit.edu; dgander@mit.edu.

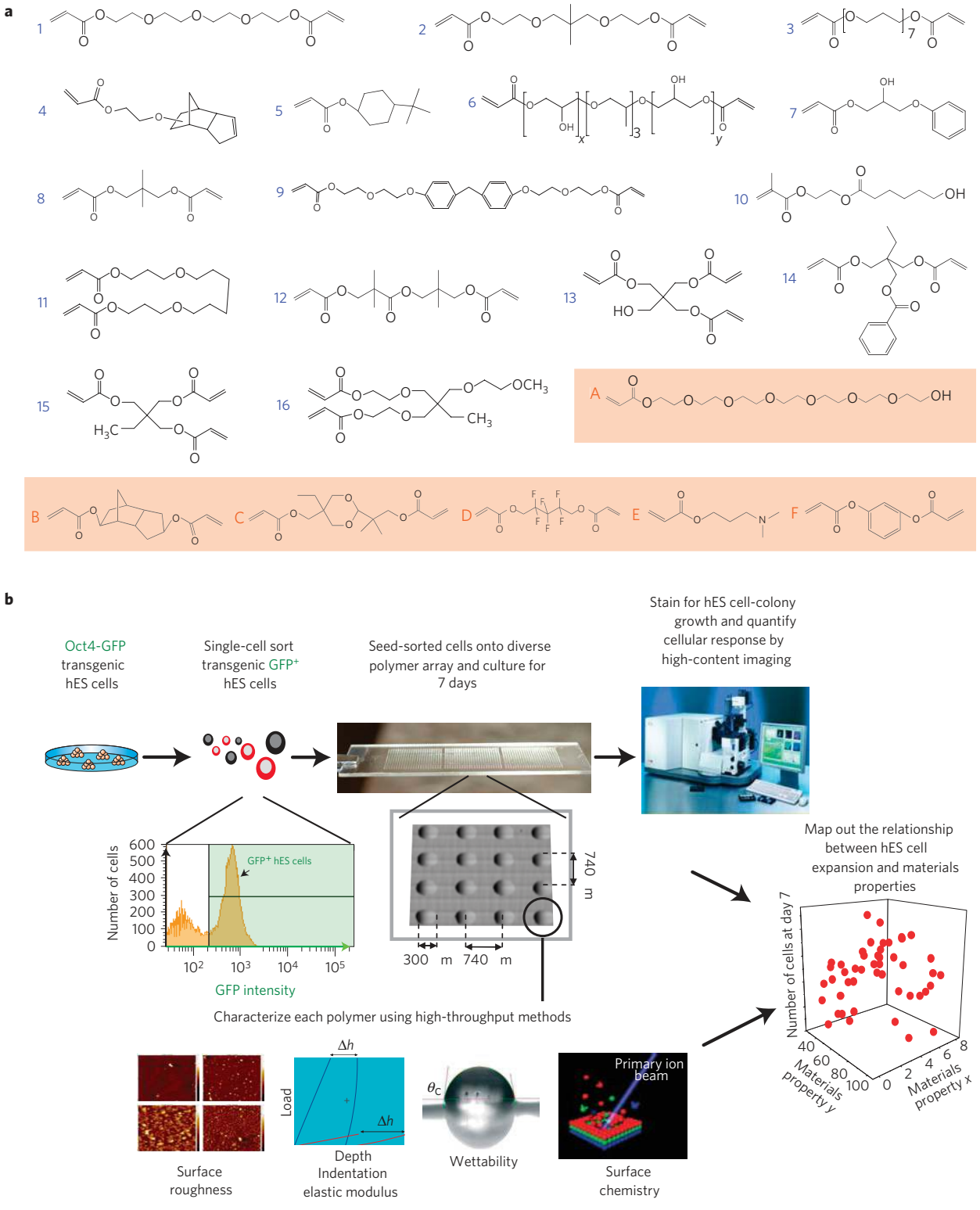

Figure 1 | High-throughput screening of biomaterials for clonal growth. a, Monomers used for array synthesis were classified into two categories: 'major' monomers that constitute >50% of the reactant mixture and 'minor' monomers that constitute <50% of the mixture. Sixteen major monomers were named numerically (blue), and six minor monomers were labelled alphabetically (orange). **b**, Schematic diagram of the screen. First, transgenic Oct4-GFP hES cells were maintained on mEFs. Then flow cytometry enabled the isolation of high-purity undifferentiated hES cells from the completely dissociated coculture of hES cells and mEFs. A flow-cytometry histogram during a representative cell sort is shown. GFP^+ cells (right of the black gate) were seeded onto the arrays, whereas the differentiated cells and mEFs (GFP^-, left of the black gate) were not used. A photograph of the polymer microarray with 16 polymer spots is shown to illustrate dimensions and separation. Each polymer was also characterized using high-throughput methods to characterize its surface roughness, indentation elastic modulus, wettability (water contact angle, θ_C) and surface chemistry. Finally, the cellular response on the polymer array was quantified by using laser-scanning cytometry, and structure–function relationships were determined by numerical analysis of both the cellular response and materials characterization data.

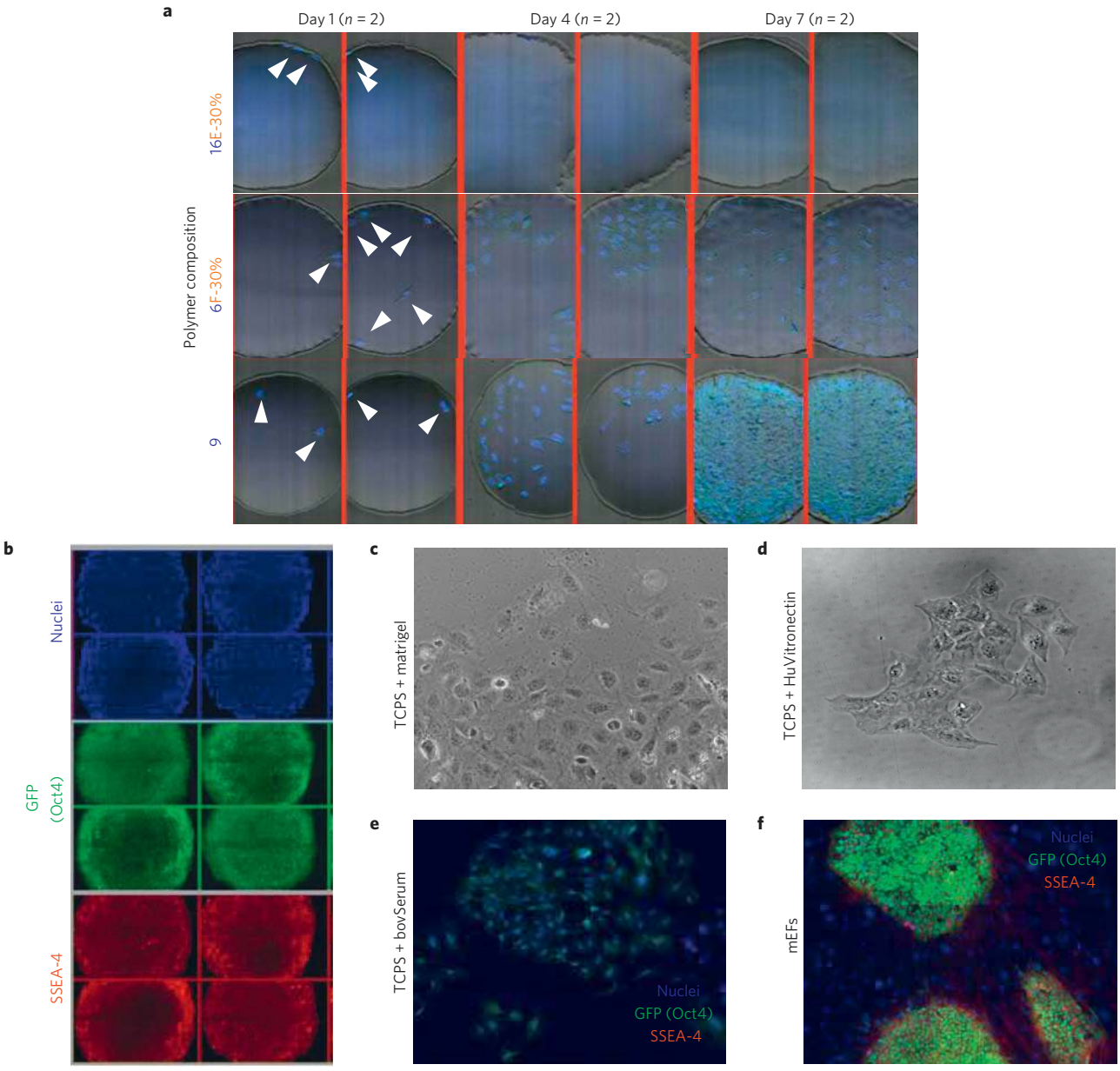

Figure 2 | Diverse hES cell behaviour on primary polymer arrays. a, Single Oct4-GFP^{+} hES cells were seeded on the polymer arrays. White arrowheads point to cells attached after one day of culture, indicating a near-clonal seeding density for each spot. Diverse cell behaviour was seen on the array on subsequent culture in mEF-conditioned media. Representative images of cell nuclei (stained by Hoechst in blue) on three different polymers (shown are two replicates of each): the 16E-30% polymer did not support either attachment or survival of dissociated hES cells; the 6F-30% polymer supported moderate growth but also differentiation of hES cells; the 9 homopolymer (a hit polymer) supported robust growth of hES cells. **b**, Immunostaining of hES cells propagated on hit polymer spots for cell nuclei (blue) and for pluripotency markers Oct4 (green) and SSEA4 (red). Owing to the raised centre of each spot above the plane of the microscope slide, spot centres are not completely in focus, leading to lower intensity at the centre of each image. **c**–**e**, At the near-clonal cell densities used for the polymer experiments, hES cells spread out on matrigel-coated tissue culture polystyrene (TCPS) (**c**), human vitronectin-coated TCPS (**d**) and bovine serum-coated TCPS (**e**) substrates in mEF-conditioned media. **f**, In contrast, traditional means of culturing hES cells by using mitotically inactivated mouse embryonic feeder cells grown on gelatin-coated TCPS ('mEFs') could support colony formation at these near-clonal cell densities. In **e** and **f** immunostaining was carried out for nuclei (blue) and for pluripotency markers Oct4 (green) and SSEA-4 (red). See also Fig. 6a for colony-formation efficiencies.

single cells (Fig. 1b, Supplementary Fig. S3) were seeded onto the polymer arrays and cultured with mEF-conditioned medium, because soluble growth factors secreted by mEFs help maintain the undifferentiated hES cell state[7,17] (Supplementary Fig. S2c).

Proteins can rapidly adsorb onto the surfaces of materials used for cell culture[26–28]. The surface properties of cell-culture substrates can modulate both the amount and the conformation of adsorbed proteins, and thereby interact with cell surface receptors (for example, integrins) to initiate signal transduction and alter cell behaviour[29]. To investigate the potential of different adsorbed proteins, fibronectin, laminin, bovine serum albumin, and fetal bovine serum (FBS) were separately adsorbed onto the microarrays from solution. In general, FBS was found to most effectively support the propagation of hES cells across the entire array, whereas fibronectin and laminin coatings led to more differentiation as indicated by down-regulation of Oct4–GFP expression (Supplementary Fig. S4).

Figure 3 | Mapping hES cell behaviour to polymer properties using primary arrays. a, Map of hES cell-colony formation and polymer composition for all of the 496 monomer combinations in the primary array. For the minor and major composition axes, the numbers and letters indicate the major and minor monomer, respectively, as shown in Fig. 1a. Major monomers are listed in order, from left to right, of increasing colony formation, and minor monomers are listed in order of increasing colony formation from bottom to top. Therefore, the region of the map corresponding to highest colony formation is the top right corner, and the region with the lowest is the bottom left corner. Homopolymers are listed on the top row. The frequency of colony formation on the primary polymer array was grouped into four categories, 0–0.25, 0.25–0.50, 0.50–0.75 and 0.75–1.0 per polymeric spot, as indicated by the intensity of red. **b**, Surface roughness of primary array polymers coated with FBS in DMEM. A map indicating the root-mean-square roughness (see coloured legend below) for all of the 496 monomer combinations in the primary array. **c**, Indentation elastic modulus of primary array polymers hydrated in PBS. A map indicating the indentation elastic modulus (see the coloured legend below) for all of the 496 monomer combinations in the primary array. Grey indicates no data obtained. **d**, Wettability of primary array polymers. A map indicating the water contact angle (see coloured legend below) for all of the 496 monomer combinations in the primary array. Note that polymers in the upper right corner of **a** with higher colony-formation frequencies (dark red) have moderate water contact angles (black) in the upper right corner of **d**, whereas this region does not correlate to any specific ranges of roughness or elastic modulus in the upper right corners of **b** and **c**.

Poor cell attachment was observed when arrays were coated with bovine serum albumin. Therefore, FBS was used initially to coat the polymer array to screen for the suitable polymers ('hits') that can support hES cell growth from single cells.

The FBS-coated arrays were seeded at low cell density (40 cells mm^{-2}), to best model the ability of cells to grow in isolation. Two to ten non-contacting cells were observed on most polymer spots after 24 h cell culture (see, for example, Fig. 2a and Supplementary Fig. S5). At various time points during culture, adherent cells were fixed and stained for cell nuclei and two pluripotent stem cell markers, SSEA-4 and Oct4 (Fig. 2b). The cellular responses were quantified with laser scanning cytometry[30]. For each polymer, we defined the colony-formation frequency as the number of polymer spots on which $Oct4^+$ and $SSEA\text{-}4^+$ hES cell colonies formed divided by the total number of replicate spots of the same kind of polymer on each array ($n = 3$–18; see Methods). After 7 days of culture, a range of cellular responses was found on the polymer array (Fig. 2a): some polymers did not

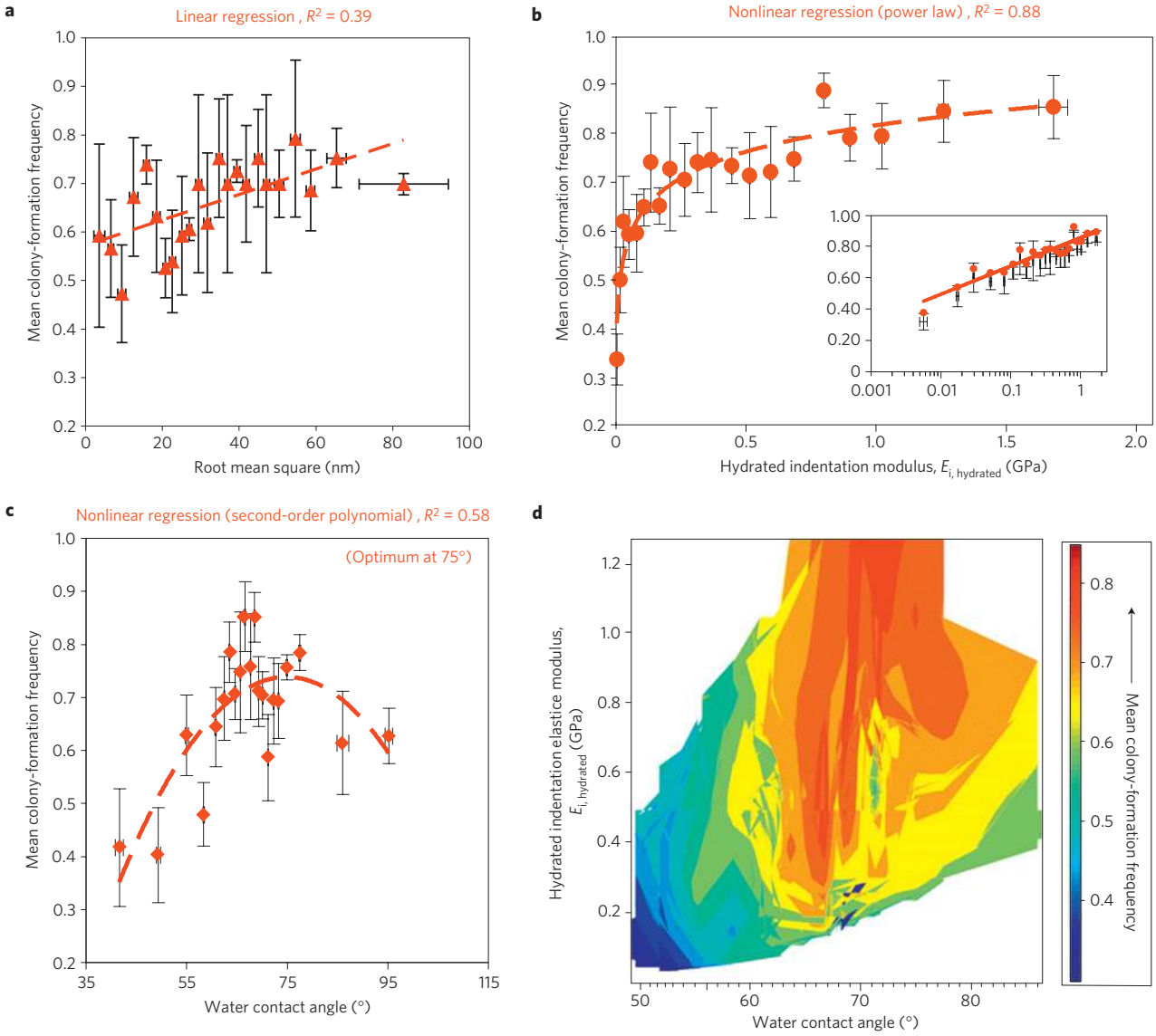

Figure 4 | Correlating hES cell behaviour to polymer properties using primary arrays. a–d, Using data in Fig. 3, regression was carried out for two properties listed at the top of each plot: colony formation versus polymer roughness (**a**), colony formation versus polymer indentation elastic modulus in the hydrated state (**b**), colony formation versus polymer wettability (**c**) and colony formation as a function of both polymer wettability and indentation elastic modulus in the hydrated state (**d**). After carrying out linear regression, second-order polynomial regression and power-law regression, only the regression with the highest R^2 is shown in each plot (dashed line). The inset in **b** is in semi-log format to indicate the behaviour at low modulus values. Data are sorted into groups of 20–25 spots as a function of increasing WCA, roughness or modulus. For the contour plot, interpolation between data points (groups of 20–25 spots) was carried out in Matlab (see Methods). In **a–c**, abscissa error bars represent the standard error of the WCA, roughness or modulus for a given group of 20–25 spots, and ordinate error bars represent the standard error of the mean of the colony-formation frequency of three replicates for a given group.

support either survival or growth of dissociated hES cells, some polymers supported the moderate growth of $Oct4^-$ differentiating cells and potential 'hit' polymers supported both robust growth and hES cell-colony formation (see also Supplementary Fig. S6). These differences in cell response demonstrate that polymers can strongly modulate hES cell behaviour between days 1 and 7 during colony growth from individual cells.

To better understand the relationship between polymer chemical composition and clonal growth of hES cells, a map of colony-formation frequency on the FBS-coated arrays against polymer monomeric composition has been generated. In Fig. 3a, major monomers are organized in order, from left to right, of increasing colony formation, and minor monomers are organized from bottom to top in order of increasing colony formation. This map indicates that the homopolymer formed from monomer 5 poorly supported clonal growth of hES cells, whereas most other homopolymers effectively supported cell growth. Tertiary amine containing minor monomer E and oligo(ethylene glycol) containing minor monomer A negatively influenced colony-formation frequency (bottom half of Fig. 3a), whereas minor monomers B, D and F could robustly support colony formation.

We characterized all polymeric substrates in the library using high-throughput techniques[31] to quantify several material properties: surface roughness (in air, PBS and culture medium after FBS adsorption), indentation elastic modulus (in air and fully hydrated in PBS) and surface wettability (Fig. 3b–d; Supplementary Fig. S7). Surface roughness and elastic properties of bulk material substrata

can affect the behaviour of adult somatic and stem cells[32–34]. Surface wettability, indicating the hydrophobicity–hydrophilicity of the polymer surface (quantified as water contact angle, WCA), has been correlated previously with protein adsorption and cell adhesion[35]. To develop quantitative relationships between the colony formation and material properties, we attempted to correlate these properties with colony-formation frequency using linear and nonlinear regression (Fig. 4, where polymer spots of distinct composition are clustered as a function of the property indicated on each horizontal axis). These data indicate that polymer surface roughness in air (root mean square, RMS ~ 0–25 nm; Supplementary Fig. S7a), in PBS (RMS ~ 0–50 nm; Supplementary Fig. S7b) and in culture medium after FBS adsorption (RMS ~ 0–110 nm; Fig. 4a) did not correlate strongly with colony-formation frequency. The standard error of measurement of material properties was low for replicate samples (for example, for WCA, < 0.9–6.9% in Supplementary Fig. S8), such that error-bar heights in Fig. 4a are indicative of this weak correlation of roughness with colony formation frequency. In contrast, a positive power-law correlation was observed between the indentation elastic modulus, E_i, of hydrated polymers and colony-formation frequency (Fig. 4b, inset). However, we note that polymers exhibiting a low indentation elastic modulus (that is, high elastic compliance) also exhibited a low WCA (Supplementary Fig. S9a). Many of these highly compliant polymers contain hydrophilic major monomer 10 and hydrophilic minor monomer A (Supplementary Fig. S10a), which is consistent with our observation that the most compliant of these hydrated polymers also exhibited the greatest change in E_i between the dry and fully hydrated states (Supplementary Fig. S9b). This trend is consistent with previous studies of cell adhesion and proliferation capacity on swellable polymers, where decreased elastic stiffness correlated directly with increased absorption of aqueous solvents[36]. Thus, the power-law correlation between E_i and colony-formation frequency (Fig. 4b) probably reflects the extent of polymer hydrophobicity–hydrophilicity in the cases where a hydrophilic polymer swells to create a compliant surface ($E_i < 0.2$ GPa) that poorly supports colony formation. Figure 4b also demonstrates that, for the present array of hydrated polymers, colony formation is not strongly governed by polymer stiffness for E_i exceeding 0.2 GPa. In contrast, a moderate wettability (WCA ~ 70°) is associated with optimal frequency of hES cell-colony formation (Fig. 4c). A contour projection of colony-formation frequency as a function of both E_i and WCA (Fig. 4d) shows clearly that the optimum wettability (65° < WCA < 80°) persists over a broad range of polymer stiffness, even for $E_i > 0.2$ GPa (see three-dimensional plot in Supplementary Fig. S10b). Thus, together these data indicate that colony-formation frequency of hES cells can be modulated more strongly by the wettability of these polymers than by variation in the elastic moduli of these polymers over the range considered.

To further refine our understanding of how this combination of material properties modulates colony formation, 48 polymers were selected to generate a 'secondary' polymer array with 36 replicates. This secondary array was designed to encompass a range of WCA similar to the range in the primary array (Supplementary Fig. S11), and the presence of 12 times more replicates significantly decreased experimental error. In good agreement with the primary-array data, a moderate wettability (WCA ~ 70°) again effectively supported optimal hES cell clonal growth (Supplementary Figs S11–S13). Surfaces of all polymers in the secondary array were analysed using time-of-flight secondary-ion mass spectrometry (ToF-SIMS) in a high-throughput manner to provide molecular information on the topmost layers (~10 Å) of each polymer surface[37,38]. ToF-SIMS spectra from two homopolymers generated from similar monomers, 1 and 16 (Fig. 5a), were substantially different, suggesting that the polymer surface chemistry cannot be necessarily predicted from the monomer composition alone. Using a chemometric technique (partial least-squares (PLS) regression on ToF-SIMS spectra)[31,38], we correlated surface chemistry contained in the spectra to the colony-formation frequency observed on each polymer in the secondary array (Fig. 5b). Good agreement between measured colony-formation frequency and that predicted from the ToF-SIMS spectra was found ($R^2 = 0.78$). Each secondary ToF-SIMS ion associated with functionalities in the polymer structures could be listed with its regression coefficient, α, a quantitative measure of its contribution to colony-formation frequency (Fig. 5b and Supplementary Fig. S14a). The tertiary-amine moiety (characteristic ions $C_3H_8N^+$, $C_2H_6N^+$, CN^-) and tertiary-butyl moiety ($C_4H_9^+$) were identified by the PLS analysis to be correlated most strongly with a low colony-formation frequency, and hydrocarbon ions ($C_2H_3^+$, $C_3H_3^+$), oxygen-containing ions (CHO_2^-, $C_3H_3O^+$, $C_2H_3O^+$) from esters and ions from cyclic structures (C_6H^-, C_4H^-, C_2H^-) had the largest effect on promoting colony formation. The oxygen-containing ions and hydrocarbon ions can be attributed to the acrylate groups ($CH_2=CHCO_2^-$) in each monomer, which form the backbone chain and the pendant ester groups after polymerization. Monomers with di- and tri-acrylates, which contain the most acrylate groups in our library, indeed showed the highest colony-formation frequencies.

The refined quantitative relationships among surface chemical structure and hES cell clonal growth generated from the secondary array provide an integrated view of all the cell responses seen on the primary array. On the primary array, the pendent functional groups in mono-acrylates (4, 5, 7 and 10) have sizeable effects on colony formation (Fig. 3a). For instance, the presence of tertiary butyl, a large non-polar functional group ($\alpha < 0$, Fig. 5b), in the major monomer 5 resulted in low colony formation. For most di- and tri-acrylate major monomers (1, 2, 8, 9, 11, 12, 13, 14 and 15) in the primary array, high acrylate content supported robust clonal formation (Fig. 3a), as expected from the large positive α (Fig. 5b). The exceptions (3, 6 and 16) can be attributed to the presence of a long chain of propylene glycol or ethylene glycol (for glycols, $\alpha < 0$, Fig. 5b). Although the ethylene glycol moiety can be found in the monomer chemistry of other di-acrylate major monomers such as 1, 2, 9 and 11, ToF-SIMS analysis indicated much higher propylene/ethylene glycol content present at the surface of homopolymers 3, 6 and 16 compared with 1, 2, 9 and 11 (Fig. 5a; Supplementary Fig. S14b). Further, the PLS model based on the secondary-array data was used to predict hES cell-colony formation of all 16 homopolymers in the primary array entirely on the basis of their ToF-SIMS spectra ($R^2 = 0.7$, Fig. 5b). This demonstrates that the model can be used to quantitatively predict hES cell clonal growth on a variety of acrylate polymers outside the training set of the model[39].

As polymers with a moderate WCA generated from multiple-acrylate-group-containing monomers performed best in these experiments, we chose the homopolymer of monomer 9, a di-acrylate with phenyl groups, and the 15A–30% copolymer, a tri-acrylate, to further validate the screening results. We fabricated 'hit arrays' where the entire polymer array is composed of one 'hit' polymer (that is, 9 or 15A-30%). The colony-formation efficiency of mEFs and hit polymer spots was quantified on the basis of the ratio of hES cell colonies formed on day 7 per attached hES cell on day 1 (Fig. 6a). About 20–25% of attached hES cells on day 1 created GFP^+, $SSEA4^+$ undifferentiated hES cell colonies after 7 days of culture on either the mEFs substrate or on the hit polymers. In contrast, cells on vitronectin- and matrigel-coated tissue-culture polystyrene (TCPS) exhibited predominantly differentiated growth, had lower Oct4 expression (similar to Fig. 2e) and did not form typical hES cell colonies with distinct borders (Fig. 2c–d). Further, nearly all (>95%) spots on hit arrays can support the expansion of $Oct4^+$, $SSEA\text{-}4^+$, $Nanog^+$ and $Tra\text{-}1\text{-}60^+$ cells after 7 day culture

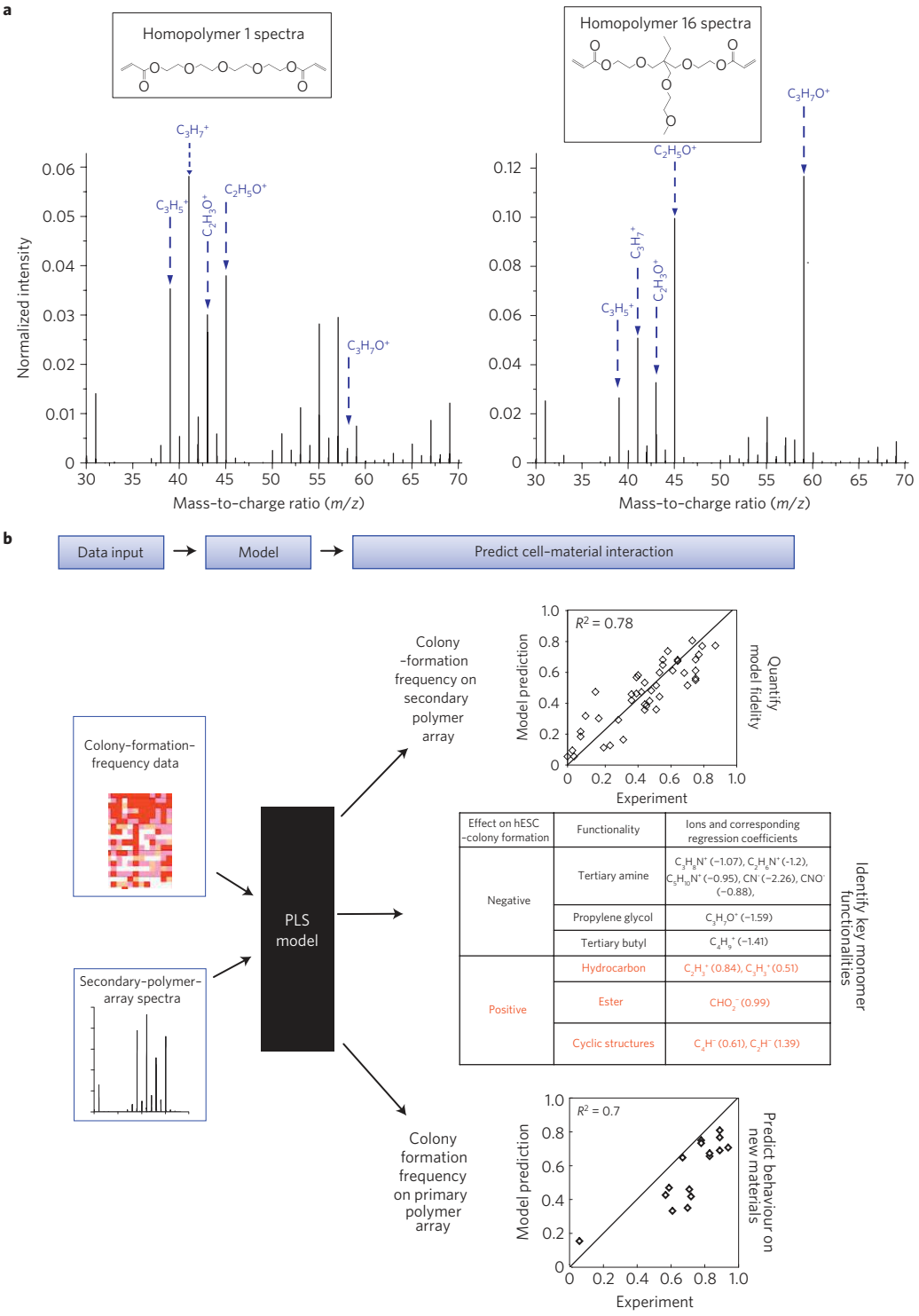

Figure 5 | Mapping cell behaviour to surface chemistry using secondary arrays. a, ToF-SIMS spectra of homopolymers 1 and 16, indicating that the surface chemistry cannot necessarily be predicted from the monomer chemistry; *m* denotes the mass and *z* denotes the charge. Arrows delineate higher intensities of hydrocarbon secondary ions ($C_3H_5^+$, $C_3H_7^+$) and ester ions ($C_2H_3O^+$) in the homopolymer 1 spectra. In contrast, higher intensities of ethylene glycol ions ($C_2H_5O^+$) and propylene glycol ions ($C_3H_7O^+$) were observed in the homopolymer 16 spectra. See the full analysis of ToF-SIMS spectra in Supplementary Fig. S14. **b**, A multivariate PLS regression method was used to quantitatively analyse and predict the cell–material interactions by correlating ToF-SIMS spectra of polymer spots to their biological performance (colony-formation frequency). The fidelity of PLS models can be quantified by a linear correlation of predicted versus measured colony-formation frequency. Top: each point in the figure represent one of 48 different polymers in the secondary array, and the inserted line represents the ideal situation when prediction match experiments completely. All ions and their regression coefficients, α, are listed in Supplementary Fig. S14a. Middle table: functionalities and their associated characteristic ions supporting or inhibiting hES colony formation. Ions were identified by correlating ToF-SIMS spectra to hES colony formation using PLS regression. Each ion was designated with a regression coefficient, α, that characterizes the relative effect on hES cell-colony formation. Bottom: as in top plot, but the PLS model was developed on ToF-SIMS spectra from the secondary array (with α values listed in the middle table) and was used to predict behaviour in the primary array.

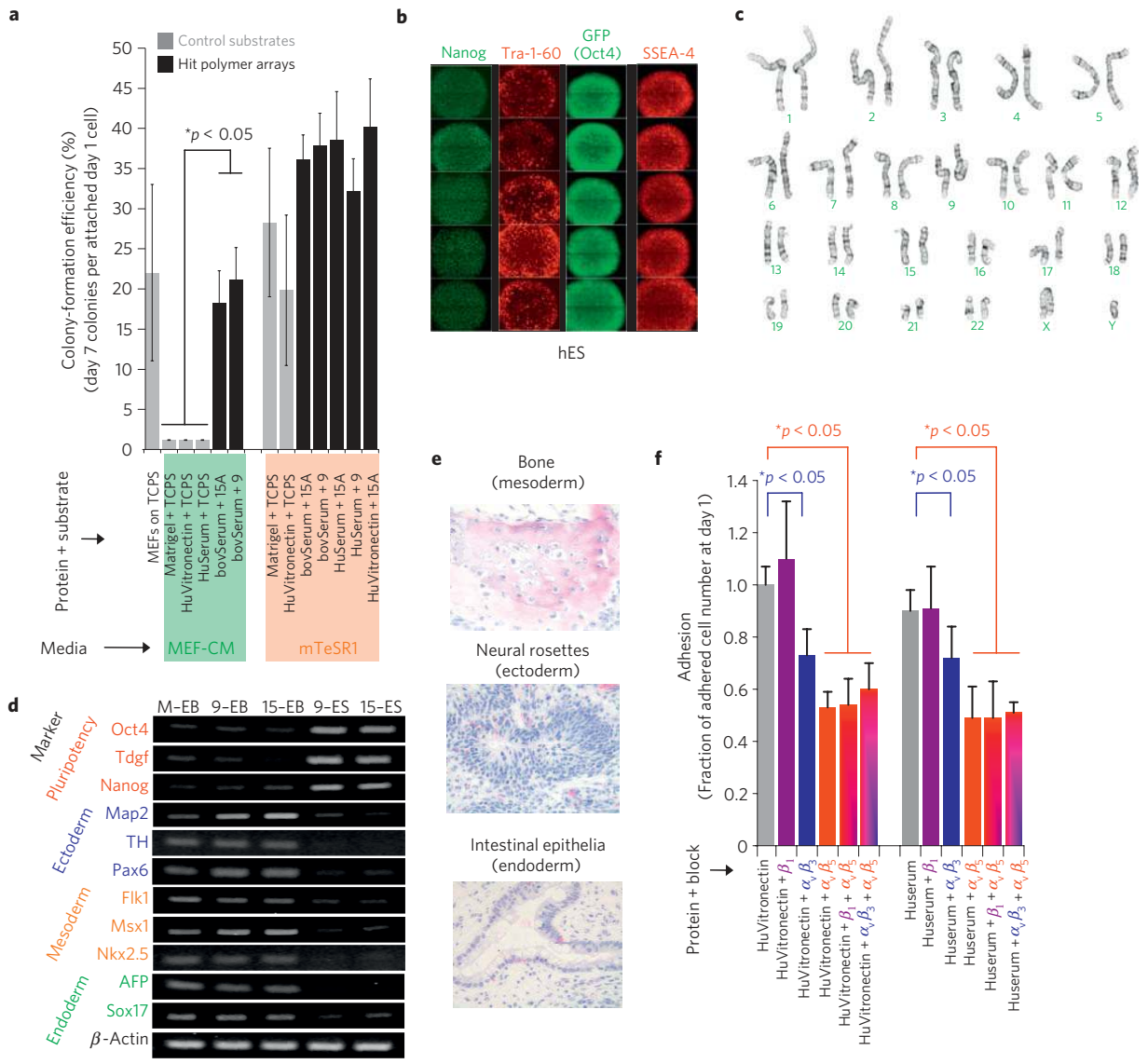

Figure 6 | Short- and long-term feeder-free culture on hit polymer arrays. a, Efficiencies of various culture systems to support undifferentiated growth of dissociated hES cells. Two medium conditions were used, labelled at the bottom: mEF-conditioned medium (MEF-CM) or chemically defined medium (mTeSR1). Several combinations of substrate and protein coating were used in conjunction with these media. Three substrates consisted of tissue culture polystyrene (TCPS), hit-polymer 9 (9; see Fig. 1a for monomer structure) and hit polymer 15A-30% (15A; see Fig. 1a for monomer structures). Four protein coatings consisted of matrigel, bovine serum, human serum and human vitronectin. Last, mEFs on gelatin-coated TCPS in regular hES medium were also used. In each condition, efficiencies were calculated as the number of SSEA-4$^+$ and Oct4$^+$ colonies seen on day 7 normalized to the number of cells attached on day 1. This metric specifically reflects the ability of substrates to promote undifferentiated clonal cell growth after correcting for any differences in initial cell attachment. **b**, Immunostaining of dissociated hES cells propagated on hit FBS-coated 15A-30% polymer for 7 days against Nanog (green) and Tra-1-60 (red), and on FBS-coated hit 9 polymer for 7 days against Oct4 (green) and SSEA-4 (red). **c**, Karyotypic analysis of hES cells propagated on hit 9 polymer array for more than 2 months (>10 passages). A normal 46XY karyotype was maintained on the hit array. **d**, Gene-expression analyses through RT-PCR of various differentiation markers for the three germ layers generated through embryoid-body (EB) *in vitro* differentiation. Lane labels are as follows: 'M-EB' for EBs generated from hES cells cultured on mEFs, '9-EB' and '15-EB' for EBs generated from hES cells cultured on 9 and 15A-30% hit polymer arrays respectively and '9-ES' and '15-ES' for hES cells cultured on 9 and 15A-30% hit polymer arrays respectively. **e**, Teratoma formation in immunodeficient mice by cells cultured on 15A-30% hit arrays. H and E staining was carried out on the teratoma. The resulting teratoma contained tissues representing all three germ layers: ectoderm, epidermal and neural tissue (rosette); mesoderm, bone and cartilage; and endoderm, respiratory epithelium and intestinal-like epithelium. **f**, Fraction of adhered cells after 24 h of culture in mTeSR1 media on hit polymer arrays coated with either human serum (HuSerum) or human vitronectin (HuVitronectin) and with the specified integrin-blocking antibody. Cell numbers shown here are averages of 24 replicates of the following hit polymers: 15, 15B-10%, 15B-20%, 15B-25%, 15D-10 and 15D-20%. β_1 blocking had minimal effect either alone or in combination with $\alpha_v\beta_5$ and $\alpha_v\beta_3$ blocking, whereas both $\alpha_v\beta_5$ and $\alpha_v\beta_3$ blocking reduced adhesion.

from completely dissociated hES single cells (Fig. 6b), and similar behaviour was seen with other pluripotent cell lines: an hiPS cell line (Supplementary Fig. S15a,b) and a non-transgenic hES cell line (Supplementary Fig. S15c,d).

The hit arrays were further evaluated for their capacity to maintain pluripotency of hES cells after more than 2 months of culture (>10 passages). Cells after prolonged culture were found to maintain an undifferentiated state with robust expression

of hES cell markers, Oct4, Nanog, Tra-1-60 and SSEA-4 (as in Fig. 6b). Clonal efficiency of cells after long-term culture remained ~20%. In addition, cells could be passaged immediately to mEFs (Supplementary Fig. 16a), and such immediate attachment and growth suggests that the hit polymers do not select for a rare subpopulation in parental culture. Additionally, a normal karyotype showed the capacity of both 'hit' polymers (9 and 15A-30%) to support genomic stability of hES cells after a long-term culture (Fig. 6c). Gene-expression results (Fig. 6d) confirmed robust differentiation of these hES cells into all three germ lineages after 13 days of EB cultivation, and derivatives of all three embryonic germ layers were seen in teratoma assays (Fig. 6e). These results demonstrate that hES cells cultured on the polymeric hits maintain their full pluripotent potential.

To develop a more clinically relevant, defined culture system for hES cells, long-term culture was conducted on human-serum-(HS-) coated hit polymer arrays in mTeSR1 medium, a completely chemically defined medium (Supplementary Fig. S17). HS-coated hit polymer arrays supported the expansion of dissociated hES cells in a similar manner to arrays coated with FBS (Fig. 6a). Further, the HS-coated hit arrays could support long-term culture for more than 1 month (>5 passages), with robust expression of hES cell markers (Supplementary Fig. S16b). Last, the HS-coated hit polymers could support the undifferentiated growth of hiPS and other hES cell lines (Supplementary Fig. S15).

To investigate the potential pathways through which human serum may be important for colony formation, we carried out blocking experiments of several highly expressed integrins on the hES/hiPS cell surface (Fig. 6f). Although there are multiple integrins on the hES cell surface that can interact in a complex manner to promote cell adhesion and self-renewal[40,41], blocking the vitronectin-binding integrins, $\alpha_v\beta_3$ and $\alpha_v\beta_5$, resulted in a significant decrease in day 1 cell adhesion, whereas blocking a matrigel-binding integrin[41], β_1, had no effect. Vitronectin is also abundantly present in serum[42], and we tested its capacity to support colony formation when coated on the hit polymers. Similar levels of hES cell adhesion at day 1 were observed on HS-coated and vitronectin-coated hit polymers (Fig. 6f). Colony-formation efficiency at day 7 on FBS/HS-coated hit polymer arrays was identical to the efficiency on vitronectin-coated hit polymers (Fig. 6a). The histogram of the cell number on the polymer spots at day 1 (Supplementary Fig. S5c) indicated that most colonies formed at day 7 are expanded from a single cell. Although vitronectin-coated TCPS was recently reported to support the culture of hES cells[9], these surfaces were not demonstrated to support hES cell clonal growth, and significant differentiation was observed during clonal growth (see, for example, Fig. 2d). Our results indicate that the surface chemistry of hit substrates interacts with vitronectin, which engages with proper hES cell surface receptors (integrin $\alpha_v\beta_3$ and $\alpha_v\beta_5$), to support the clonal, undifferentiated growth of human pluripotent cells.

The biological activities of polymeric substrates can be controlled by surface properties, which in turn can be determined by chemical moieties present on the polymer surface. However, it may be difficult to quantitatively predict the presence of certain chemical functional groups at the polymer surface from the monomer composition alone, as well as the effects of surface chemistry on biological performance[43]. Here we employed high-throughput material synthesis and analysis to rapidly establish quantitative models between polymer-surface chemical structures and hES cell clonal growth. Using surface chemical structure information of the adsorbed protein layer (for example, vitronectin) did not result in more predictive models of hES cell-colony formation (Supplementary Fig. S18), indicating that ToF-SIMS can resolve surface-chemistry differences on polymers leading to colony formation but is less likely to resolve protein structural information leading to colony formation. Our analysis suggests that adsorbed proteins from our initial protein coating (but potentially also from culture media or hES cell secretion) need to interact with the appropriate polymer surface chemistry to be in the proper conformation to optimally promote colony formation. In addition to surface chemistry, which was demonstrated to have a controlling effect on stem cell behaviour, the geometry of the spot may influence self-renewal of hES cells as well, potentially by enhancing autocrine or juxtacrine signalling[44,45]. Last, the combination of human-vitronectin-coated hit polymers and mTeSR1 medium provides an attractive platform to develop a fully chemically defined, xeno-free, feeder-free culture system, as the only animal component, bovine serum albumin from the mTeSR1 medium, can be replaced by human serum albumin. Together, these advances may permit the facile growth of clinically relevant hES/hiPS cells from fully dissociated single cells, thereby enabling more straightforward genetic manipulation.

Methods

Combinatorial array preparation. Polymers were printed in a humid Ar atmosphere on epoxy-monolayer-coated glass slides (Xenopore Xenoslide E, Hawthorne, New Jersey), which were first dip-coated in 4 w/v% poly(2-hydroxyethyl methacrylate), using modifications of robotic fluid-handling technology as described previously[23]. Spots were polymerized through 10 s exposure to long-wave ultraviolet radiation (365 nm), dried at <50 mtorr for at least 7 days and coated with 20% serum or other proteins. See also Supplementary Methods and Figs S1 and S11a for the composition of primary and secondary arrays.

Surface-roughness measurements. Using an atomic force microscope (Digital Instruments Dimensions 3000A) in tapping mode, 5-μm regions of each polymer were measured and the root mean squared roughness was calculated. See also Supplementary Methods.

Elastic-modulus measurements. Using a pendulum-based instrumented nanoindenter (NanoTest, Micro Materials), experiments were conducted in ambient air or using a modified platform for *in situ* liquid experiments[46]. Samples were indented with a spherical ruby indenter of radius $R = 500\,\mu m$ ($n = 3$ locations for each polymer spot) with loading and unloading rates of $0.5\,mN\,s^{-1}$, a dwell of 10 s and a maximum load of 3 mN or a maximum depth of 600 nm. Loading rates were chosen such that the reduced elastic modulus inferred from indentation could be calculated from the initial unloading slope[47,48]. The indentation elastic modulus presented in the manuscript was calculated from the measured reduced elastic modulus, assuming a Poisson's ratio of 0.49 for all polymers. See also Supplementary Methods.

Water-contact-angle measurements. Measurements were of the sessile-drop type and made using ultrapure water on a Kruss DSA 100 apparatus fitted with a piezo-doser head. See also Supplementary Methods.

Time-of-flight secondary-ion mass spectroscopy. A secondary-ion mass spectrometer (ION-TOF, IV, UK) was operated using a Bi_3^+ primary-ion source at 25 kV and in 'bunched mode'. A 1 pA primary-ion beam was rastered at an area of $100 \times 100\,\mu m$. Secondary ions were collected from the same area of each polymer spot on the microarray over 10 s acquisition time. Ion masses were determined using a high-resolution TOF analyser, and the typical mass resolution (at m/z 41) was just over 6,000.

Cell culture. hES cell lines BG01 and WIBR3 were maintained on mitomycin C-inactivated mEF feeder layers in standard medium. hES BG01–Oct4–GFP cells were made by introducing a Oct4–GFP–puro construct into hES cells[25]. hiPS C1 cells were derived through lentiviral infection of Oct4, Sox2 and Klf4 and cultured on mEFs as described previously[49]. For EB-induced differentiation, hES cell colonies were cultured for 13 days in non-adherent suspension culture dishes (Corning) in DMEM supplemented with 15% FBS.

For fluorescence-activated cell sorting, hES or hiPS cell lines were cultured in 10 μM Rho-associated kinase inhibitor (Calbiochem; Y-27632) for 24 h in standard mEF conditions before sorting. Cells were harvested enzymatically with $1\,mg\,ml^{-1}$ collagenase and then with 0.05% trypsin for 5 min at 37 °C. hiPS cells were immunostained using SSEA-4. Cells were collected in media with Rho-associated kinase inhibitor and sorted on a FACSAria Flow Cytometer (Becton Dickinson, San Jose, California). Cells were subsequently plated on various surfaces in medium supplemented with Rho-associated kinase inhibitor for the first 24 h of culture to reduce initial apoptosis of completely dissociated hES cells[50]. For HS-coated hit arrays, culturing occurred in mTeSR1 media (Stemcell Technologies). Long-term culture on hit arrays occurred in mTeSR1 media and by passaging 1:3 every 5–7 days using collagenase. See also Supplementary Methods.

Biological assays. For teratoma formation, hES cells were injected subcutaneously in the back of severe combined immunodeficient mice (Taconic) and tumours generally developed within 4–8 weeks. After sectioning, teratomas were diagnosed on the basis of haematoxylin and eosin staining. For karyotype analysis, chromosomal studies were carried out by Cell Line Genetics (Madison, Wisconsin) using standard protocols for high-resolution G-banding. For immunocytochemistry, cells were fixed in 4% paraformaldehyde in PBS and immunostained according to standard protocols. See also Supplementary Methods.

Numerical methods. Principal component analysis and PLS regression were carried out using the Eigenvector PLS_Toolbox 3.5 using the SIMPLS algorithm. For linear and nonlinear least-squares regression, Excel (Microsoft) was used. Contour and three-dimensional plots were generated in MATLAB4 (Mathworks) using the v4 griddata method of data interpolation. See also Supplementary Methods.

Efficiency measurements. Using a low (1.6 cells mm^{-2}) seeding density, day 1 cell and day 7 colony numbers on mEFs and matrigel were normalized per scanned surface area and on 'hit' polymer spots as per 'hit' array (1,875 mm^2, 1,728 replicates). For experiments on TCPS, single cells were sorted individually directly into each well of a coated 96-well plate. Day 1 cell and day 7 colony numbers were measured by manually counting stained wells. For vitronectin-coated, matrigel-coated and HS-coated TCPS in mEF-conditioned media, no GFP^+ colonies were observed: in about 30% of cases we observed only differentiated cell growth. See also Supplementary Methods.

Received 21 September 2009; accepted 24 June 2010; published online 22 August 2010

References

1. Thomson, J. A. *et al.* Embryonic stem cell lines derived from human blastocysts. *Science* **282,** 1145–1147 (1998).
2. Takahashi, K. *et al.* Induction of pluripotent stem cells from adult human fibroblasts by defined factors. *Cell* **131,** 861–872 (2007).
3. Yu, J. *et al.* Induced pluripotent stem cell lines derived from human somatic cells. *Science* **318,** 1917–1920 (2007).
4. Daley, G. Q. & Scadden, D. T. Prospects for stem cell-based therapy. *Cell* **132,** 544–548 (2008).
5. Saha, K. & Jaenisch, R. Technical challenges in using human induced pluripotent stem cells to model disease. *Cell Stem Cell* **5,** 584–595 (2009).
6. Amit, M. *et al.* Clonally derived human embryonic stem cell lines maintain pluripotency and proliferative potential for prolonged periods of culture. *Dev. Biol.* **227,** 271–278 (2000).
7. Xu, C. *et al.* Feeder-free growth of undifferentiated human embryonic stem cells. *Nature Biotechnol.* **19,** 971–974 (2001).
8. Stojkovic, P. *et al.* Human-serum matrix supports undifferentiated growth of human embryonic stem cells. *Stem Cells* **23,** 895–902 (2005).
9. Braam, S. R. *et al.* Recombinant vitronectin is a functionally defined substrate that supports human embryonic stem cell self-renewal via alphavbeta5 integrin. *Stem Cells* **26,** 2257–2265 (2008).
10. Li, Y., Powell, S., Brunette, E., Lebkowski, J. & Mandalam, R. Expansion of human embryonic stem cells in defined serum-free medium devoid of animal-derived products. *Biotechnol. Bioeng.* **91,** 688–698 (2005).
11. Amit, M., Shariki, C., Margulets, V. & Itskovitz-Eldor, J. Feeder layer- and serum-free culture of human embryonic stem cells. *Biol. Reprod.* **70,** 837–845 (2004).
12. Yao, S. *et al.* Long-term self-renewal and directed differentiation of human embryonic stem cells in chemically defined conditions. *Proc. Natl Acad. Sci. USA* **103,** 6907–6912 (2006).
13. Ludwig, T. E. *et al.* Feeder-independent culture of human embryonic stem cells. *Nature Methods* **3,** 637–646 (2006).
14. Ludwig, T. E. *et al.* Derivation of human embryonic stem cells in defined conditions. *Nature Biotechnol.* **24,** 185–187 (2006).
15. Rodin, S. *et al.* Long-term self-renewal of human pluripotent stem cells on human recombinant laminin-511. *Nature Biotechnol.* **28,** 611–615 (2010).
16. Li, Y. J., Chung, E. H., Rodriguez, R. T., Firpo, M. T. & Healy, K. E. Hydrogels as artificial matrices for human embryonic stem cell self-renewal. *J. Biomedical Mater. Res. Part A* **79,** 1–5 (2006).
17. Gerecht, S. *et al.* Hyaluronic acid hydrogel for controlled self-renewal and differentiation of human embryonic stem cells. *Proc. Natl Acad. Sci. USA* **104,** 11298–11303 (2007).
18. Villa-Diaz, L. G. *et al.* Synthetic polymer coatings for long-term growth of human embryonic stem cells. *Nature Biotechnol.* **28,** 581–583 (2010).
19. Melkoumian, Z. *et al.* Synthetic peptide–acrylate surfaces for long-term self-renewal and cardiomyocyte differentiation of human embryonic stem cells. *Nature Biotechnol.* **28,** 606–610 (2010).
20. Zou, J. *et al.* Gene targeting of a disease-related gene in human induced pluripotent stem and embryonic stem cells. *Cell Stem Cell* **5,** 97–110 (2009).
21. Hockemeyer, D. *et al.* Efficient targeting of expressed and silent genes in human ESCs and iPSCs using zinc-finger nucleases. *Nature Biotechnol.* **27,** 851–857 (2009).
22. Zwaka, T. P. & Thomson, J. A. Homologous recombination in human embryonic stem cells. *Nature Biotechnol.* **21,** 319–321 (2003).
23. Anderson, D. G., Levenberg, S. & Langer, R. Nanoliter-scale synthesis of arrayed biomaterials and application to human embryonic stem cells. *Nature Biotechnol.* **22,** 863–866 (2004).
24. Mei, Y. *et al.* Mapping the interactions among biomaterials, adsorbed proteins, and human embryonic stem cells. *Adv. Mater.* **21,** 2781–2876 (2009).
25. Green, J. J. *et al.* Nanoparticles for gene transfer to human embryonic stem cell colonies. *Nano Lett.* **8,** 3126–3130 (2008).
26. Tamada, Y. & Ikada, Y. Effect of preadsorbed proteins on cell-adhesion to polymer surfaces. *J. Colloid Interf. Sci.* **155,** 334–339 (1993).
27. Underwood, P. A., Steele, J. G. & Dalton, B. A. Effects of polystyrene surface chemistry on the biological activity of solid phase fibronectin and vitronectin, analysed with monoclonal antibodies. *J. Cell Sci.* **104,** 793–803 (1993).
28. van Wachem, P. B. *et al.* The influence of protein adsorption on interactions of cultured human endothelial cells with polymers. *J. Biomed. Mater. Res.* **21,** 701–718 (1987).
29. Keselowsky, B. G., Collard, D. M. & Garcia, A. J. Integrin binding specificity regulates biomaterial surface chemistry effects on cell differentiation. *Proc. Natl Acad. Sci. USA* **102,** 5953–5957 (2005).
30. Luther, E., Kamentsky, L., Henriksen, M. & Holden, E. *Cytometry, New Developments,* Vol. 75, 4th edn, 185–218 (2004).
31. Urquhart, A. J. *et al.* High throughput surface characterisation of a combinatorial material library. *Adv. Mater.* **19,** 2486–2491 (2007).
32. Lipski, A. M. *et al.* Nanoscale engineering of biomaterial surfaces. *Adv. Mater.* **19,** 553–557 (2007).
33. Engler, A. J., Sen, S., Sweeney, H. L. & Discher, D. E. Matrix elasticity directs stem cell lineage specification. *Cell* **126,** 677–689 (2006).
34. Saha, K. *et al.* Substrate modulus directs neural stem cell behaviour. *Biophys. J.* **95,** 4426–4438 (2008).
35. Tamada, Y. & Ikada, Y. Effect of preadsorbed proteins on cell-adhesion to polymer surfaces. *J. Colloid Inter. Sci.* **155,** 334–339 (1993).
36. Thompson, M. T., Berg, M. C., Tobias, I. S., Rubner, M. F. & Van Vliet, K. J. Tuning compliance of nanoscale polyelectrolyte multilayers to modulate cell adhesion. *Biomaterials* **26,** 6836–6845 (2005).
37. Delcorte, A. *et al.* ToF-SIMS study of alternate polyelectrolyte thin films: Chemical surface characterization and molecular secondary ions sampling depth. *Surf. Sci.* **366,** 149–165 (1996).
38. Vickerman, J. C. *ToF-SIMS: Surface Analysis by Mass Spectrometry* (IM Publications, 2001).
39. Urquhart, A. J. *et al.* TOF-SIMS analysis of a 576 micropatterned copolymer array to reveal surface moieties that control wettability. *Anal. Chem.* **80,** 135–142 (2008).
40. Meng, Y. *et al.* Characterization of integrin engagement during defined human embryonic stem cell culture. *FASEB J.* **24,** 1056–1065 (2010).
41. Rowland, T. J. *et al.* Roles of integrins in human induced pluripotent stem cell growth on matrigel and vitronectin. *Stem Cells Dev.* doi:10.1089/scd.2009.0328 (2010).
42. Hayman, E. G., Pierschbacher, M. D., Ohgren, Y. & Ruoslahti, E. Serum spreading factor (vitronectin) is present at the cell surface and in tissues. *Proc. Natl Acad. Sci. USA* **80,** 4003–4007 (1983).
43. Neuss, S. *et al.* Assessment of stem cell/biomaterial combinations for stem cell-based tissue engineering. *Biomaterials* **29,** 302–313 (2008).
44. Guilak, F. *et al.* Control of stem cell fate by physical interactions with the extracellular matrix. *Cell Stem Cell* **5,** 17–26 (2009).
45. Peerani, R. *et al.* Niche-mediated control of human embryonic stem cell self-renewal and differentiation. *EMBO J.* **26,** 4744–4755 (2007).
46. Constantinides, G., Kalcioglu, Z. I., McFarland, M., Smith, J. F. & Van Vliet, K. J. Probing mechanical properties of fully hydrated gels and biological tissues. *J. Biomechanics* **41,** 3285–3289 (2008).
47. Oliver, W. C. & Pharr, G. M. An improved technique for determining hardness and elastic modulus using load and displacement sensing indentation experiments. *J. Mater. Res.* **7,** 1564–1583 (1992).
48. Cheng, Y-T. & Cheng, C-M. Scaling, dimensional analysis, and indentation measurements. *Mater. Sci. Eng.* **44,** 91–149 (2004).
49. Hockemeyer, D. *et al.* A drug-inducible system for direct reprogramming of human somatic cells to pluripotency. *Cell Stem Cell* **3,** 346–353 (2008).
50. Watanabe, K. *et al.* A ROCK inhibitor permits survival of dissociated human embryonic stem cells. *Nature Biotechnol.* **25,** 681–686 (2007).

Acknowledgements

We thank C. Beard, R. Alagappan, P. Xu, P. Wisniewski, C. Araneo, K. Wood, J. Daussman, R. Flannery, D. Fu, E. Luther and Compucyte for technical support.

We thank all the members of the Langer laboratory and Jaenisch laboratory for helpful discussions and comments on the manuscript. R.J. was supported by NIH grants R37-CA084198, RO1-CA087869 and RO1-HD045022. R.L., R.J. and D.G.A. are advisors to Stemgent and R.L. and R.J. are cofounders of Fate Therapeutics. Financial support for J.Y. and A.H. is from the Wellcome Trust 085246. K.S. is supported by the Society in Science: the Branco Weiss Fellowship. D.G.A., R.L. and Y.M. are supported by NIH DE016516. Z.I.K. was supported by the US Army through the Institute for Soldier Nanotechnologies, under Contract W911NF-07-D-0004 with the US Army Research Office.

Author contributions

All of the authors developed experiments, participated in the generation and analysis of data and assisted in the writing of the manuscript.

Additional information

The authors declare no competing financial interests. Supplementary information accompanies this paper on www.nature.com/naturematerials. Reprints and permissions information is available online at http://npg.nature.com/reprintsandpermissions. Correspondence and requests for materials should be addressed to R.L., R.J. or D.G.A.